Geophysical Journal International

Geophys. J. Int. (2016) **204,** 892–906 doi: 10.1093/gji/ggv493
GJI Gravity, geodesy and tides

Accounting for time- and space-varying changes in the gravity field to improve the network adjustment of relative-gravity data

Jeffrey R. Kennedy[1,2] and Ty P.A. Ferré[2]

[1] *U.S. Geological Survey, Arizona Water Science Center, Tucson, AZ* 85719*, USA. E-mail: jkennedy@usgs.gov*
[2] *Department of Hydrology and Water Resources, University of Arizona, Tucson, AZ* 85721*, USA*

Accepted 2015 November 9. Received 2015 November 6; in original form 2015 August 27

SUMMARY

The relative gravimeter is the primary terrestrial instrument for measuring spatially and temporally varying gravitational fields. The background noise of the instrument—that is, non-linear drift and random tares—typically requires some form of least-squares network adjustment to integrate data collected during a campaign that may take several days to weeks. Here, we present an approach to remove the change in the observed relative-gravity differences caused by hydrologic or other transient processes during a single campaign, so that the adjusted gravity values can be referenced to a single epoch. The conceptual approach is an example of coupled hydrogeophysical inversion, by which a hydrologic model is used to inform and constrain the geophysical forward model. The hydrologic model simulates the spatial variation of the rate of change of gravity as either a linear function of distance from an infiltration source, or using a 3-D numerical groundwater model. The linear function can be included in and solved for as part of the network adjustment. Alternatively, the groundwater model is used to predict the change of gravity at each station through time, from which the accumulated gravity change is calculated and removed from the data prior to the network adjustment. Data from a field experiment conducted at an artificial-recharge facility are used to verify our approach. Maximum gravity change due to hydrology (observed using a superconducting gravimeter) during the relative-gravity field campaigns was up to 2.6 μGal d^{-1}, each campaign was between 4 and 6 d and one month elapsed between campaigns. The maximum absolute difference in the estimated gravity change between two campaigns, two months apart, using the standard network adjustment method and the new approach, was 5.5 μGal. The maximum gravity change between the same two campaigns was 148 μGal, and spatial variation in gravity change revealed zones of preferential infiltration and areas of relatively high groundwater storage. The accommodation for spatially varying gravity change would be most important for long-duration campaigns, campaigns with very rapid changes in gravity and (or) campaigns where especially precise observed relative-gravity differences are used in the network adjustment.

Key words: Time variable gravity; Hydrogeophysics; Hydrology.

1 INTRODUCTION

Despite advances in instrumentation, it remains difficult to rapidly collect accurate terrestrial gravity data over large areas. The practitioner can employ portable absolute gravimeters (namely, the Micro-g Lacoste, Inc., A-10 gravimeter; Brown *et al.* 1999; Ferguson *et al.* 2007), relative gravimeters (such as the Scintrex Ltd.. CG-5 meter and the ZLS Corp. Burris meter), or both. But their size, limited mobility, power requirements, cost and the time required for observations limit applications for many studies. The last factor, time, is perhaps most limiting; 20 stations per day per instrument (operator) is an ambitious goal for any study and five or less is not unusual. If the timescale of the hydrologic or other transient process of interest leads to measurable changes in gravity over the duration of a field campaign, temporal changes will be merged with spatial variations in gravity, potentially leading to misinterpretations of the processes under investigation (throughout, 'campaign' refers to the set of measurements used in a network adjustment, whereas 'survey' refers to the set of measurements for which a single drift correction applies, typically collected on a single day. Campaigns will typically comprise several surveys).

The zero-length-spring relative gravimeter continues to be the standard field instrument for measuring spatially variable gravity fields. The fundamental design of this instrument dates to the 1930s

(LaCoste 1988), and low-frequency drift and tares, or offsets, are always present even in modern instruments. Thanks to proper field procedures, however, they have proven widely applicable for time-lapse hydrology (e.g. Pool, 2008; Jacob *et al.* 2010; Christiansen *et al.* 2011a,b; Pfeffer *et al.* 2013), volcanology (e.g. Bonvalot *et al.* 1998; Battaglia *et al.* 2008) and oil and gas investigations (e.g. Alnes *et al.* 2008). This paper extends the use of relative gravimeters and the network adjustment of survey data to measure, for the first time, a spatially variable gravity field that is changing at a rate faster than observations can be made across the entire network of stations. To do so, the gravity rate of change at each station is modelled explicitly using either a linear model of the gravity rate of change as a function of distance from an infiltration source, or a numerical groundwater model.

The primary method of collecting time-lapse gravity data over a network of stations is to observe all of the stations during a single-field campaign; the entire campaign is then repeated at a later date. A typical campaign may take days or weeks to complete. At the conclusion of each campaign, all data are combined using the least-squares network adjustment method to determine a unique gravity value at each station (Torge 1989). The datum for each campaign can be established using absolute gravimeters or superconducting gravimeters, a method called hybrid gravity (Furuya *et al.* 2003; Crossley *et al.* 2013; Hector *et al.* 2015); estimated based on local hydrology or other factors (Pool & Eychaner 1995; Gettings *et al.* 2008); or the gravity differences can be interpreted directly (Jacob *et al.* 2009; Naujoks *et al.* 2010). The change in gravity between campaigns—typically the value of interest, either as a direct estimate of mass change or for model calibration—is calculated by differencing the network-adjusted values from successive campaigns.

The major obstacles to conducting rapid gravity campaigns are inherent in the relative gravimeter. Observations at each station take five minutes or longer; combined with traveltime between stations and repeat occupations, a limited number of stations can be visited in a day. Due to low-frequency drift and tares (offsets), repeat occupations of a base station are necessary on a regular basis (Long & Kaufmann 2013). To minimize the impact of drift and tares (i.e. the always-changing, constant offset inherent in relative gravimeters), it is common to consider only the relative difference in gravity between two stations rather than the actual reading at any particular station. An additional advantage of considering gravity differences, rather than individual observations, is that for stations observed with relatively little elapsed time in between, common-mode signals such as barometric pressure changes are automatically removed (Kennedy *et al.* 2014).

Least-squares network adjustment is a common method for combining survey measurements of all types (Anderson *et al.* 1998). For gravity networks, network adjustment combines relative-gravity differences with absolute-gravity values to determine a unique gravity value and associated uncertainty at each station. The network adjustment can include model terms to account for gravimeter drift during a campaign (Hwang *et al.* 2002). In this work, we propose a new conceptual approach to adjust both time- and space-varying changes in the gravity field during a single campaign. As an example, we consider the change in gravity caused by a transient hydrologic process over the course of a single campaign. We first show that, for some scenarios, this can be modelled using a linear model, which is included directly in the network adjustment. Then, we extend our treatment to show how a more general numerical groundwater-flow model can be used to account for changes in gravity at each station at each observation time.

1.1 Observations of rapid gravity change

The development of a method to allow for monitoring in the presence of rapid gravity changes during a single campaign is motivated by a field experiment conducted from 2012 February to 2013 May at the Southern Avra Valley Storage and Recovery Project operated by the City of Tucson (Fig. 1; Kennedy *et al.* 2014). Continuous gravimeters, deployed at two locations for the duration of the study, recorded changes in gravity residuals due to hydrology among the highest ever, up to 6 μGal d^{-1} (residuals refer to the remaining gravity signal after tidal and atmospheric effects have been removed). The project operates seven basins of about 500 m^2 each that recharge water imported from the Colorado River via the Central Arizona Project Canal. The basins are flooded in cycles ranging from weeks to months. Infiltration rates range from 0.1 to 0.5 m d^{-1}, and generally increase with the duration of flooding. There are several public-supply wells nearby, the nearest of which, AV019A (Fig. 1) pumps about 8000 m^3 d^{-1} with frequent on/off cycles.

In Spring 2013, three relative-gravity campaigns were carried out on a network of 72 stations during one drainage cycle. The first campaign, with 259 observed relative-gravity differences, took place when basins RB205, RB206 and RB207 (Fig. 1) were flooded (approximately 2-m ponding height) and actively recharging. The second campaign, with 231 observed relative-gravity differences, began 22 d after the basin inflows were turned off; the basin surfaces dried within 2–3 d after inflow stopped. The third campaign, with 218 observed relative-gravity differences, began 46 d after inflow stopped. These three campaigns were conducted in February, March and April and took 5, 4 and 4 d, respectively; the first campaign was spread over 9 d and the others over consecutive days. The average gravity rate of change at RB206 for the February, March and April campaigns was 1.2 μGal d^{-1}, 2.6 μGal d^{-1} and 1.6 μGal d^{-1}, respectively; at RB207 the rate of change was 1.2 μGal d^{-1}, 1.2 μGal d^{-1} and 0.9 μGal d^{-1} for the three campaigns (the maximum rate of change during the entire experiment was 6.0 μGal^{-1} d^{-1}, during infiltration at RB206). During the approximately 2-month study period, the accumulated groundwater mound beneath the basins dissipated and water continued to percolate downward and away from the gravity stations on the land surface. A Burris relative gravimeter (B44; ZLS Corporation) was used for all observations. During the first and third campaigns, each station was surveyed using differential GPS to determine if station elevation change occurred. The average absolute elevation change was 0.004 m and the measurement accuracy of the GPS-derived elevation was about 0.01 m. Therefore, gravity change due to elevation change at all stations was considered insignificant.

1.2 Rapid gravity changes induced by ground water flow

Infiltration causes gravity change as air-filled pore spaces fill with water, increasing the bulk density of the subsurface (Pool 2008). If the infiltration source is distributed evenly across an area (e.g. rainfall) and the terrain is relatively flat, the gravity change may be modelled using the horizontal-infinite (Bouguer) slab approximation. Alternatively, linear relations (admittance factors) that account for local topography may be used (Creutzfeldt *et al.* 2008). In either case, the gravity change per unit thickness of water infiltrated is constant (42 μGal m^{-1} of water for the Bouguer slab). If the same admittance factor was valid at each station, the rate of change of gravity during a campaign owing to infiltration would be the same at each station and therefore cancel as a common-mode signal. In that

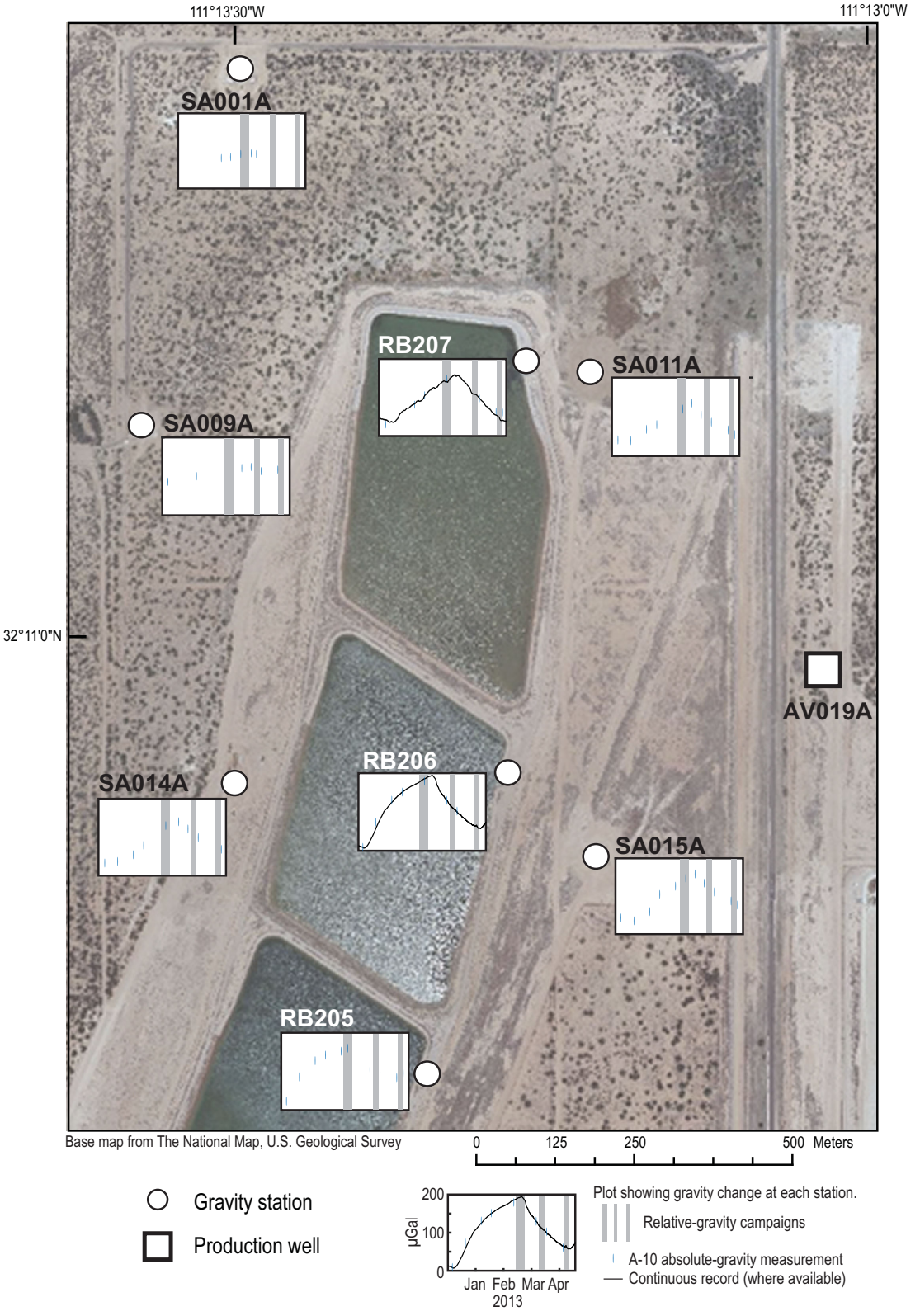

Figure 1. Map showing rapid gravity change at an artificial-recharge facility observed using an A-10 absolute gravimeter and continuous gravimeters. Continuous data at RB206 and RB207 were recorded using an iGrav superconducting gravimeters and gPhone relative gravimeter, respectively.

case, no special consideration of the hydrologic process is required in the network adjustment.

In the more general case, infiltration, drainage, evapotranspiration and the associated changes in gravity and rates of change of gravity vary in space. Evaluating the spatial dependence of the rate of change in gravity (i.e. as a function of station location) is critical to account for transient processes during network adjustment. For example, consider a simplified representation of the

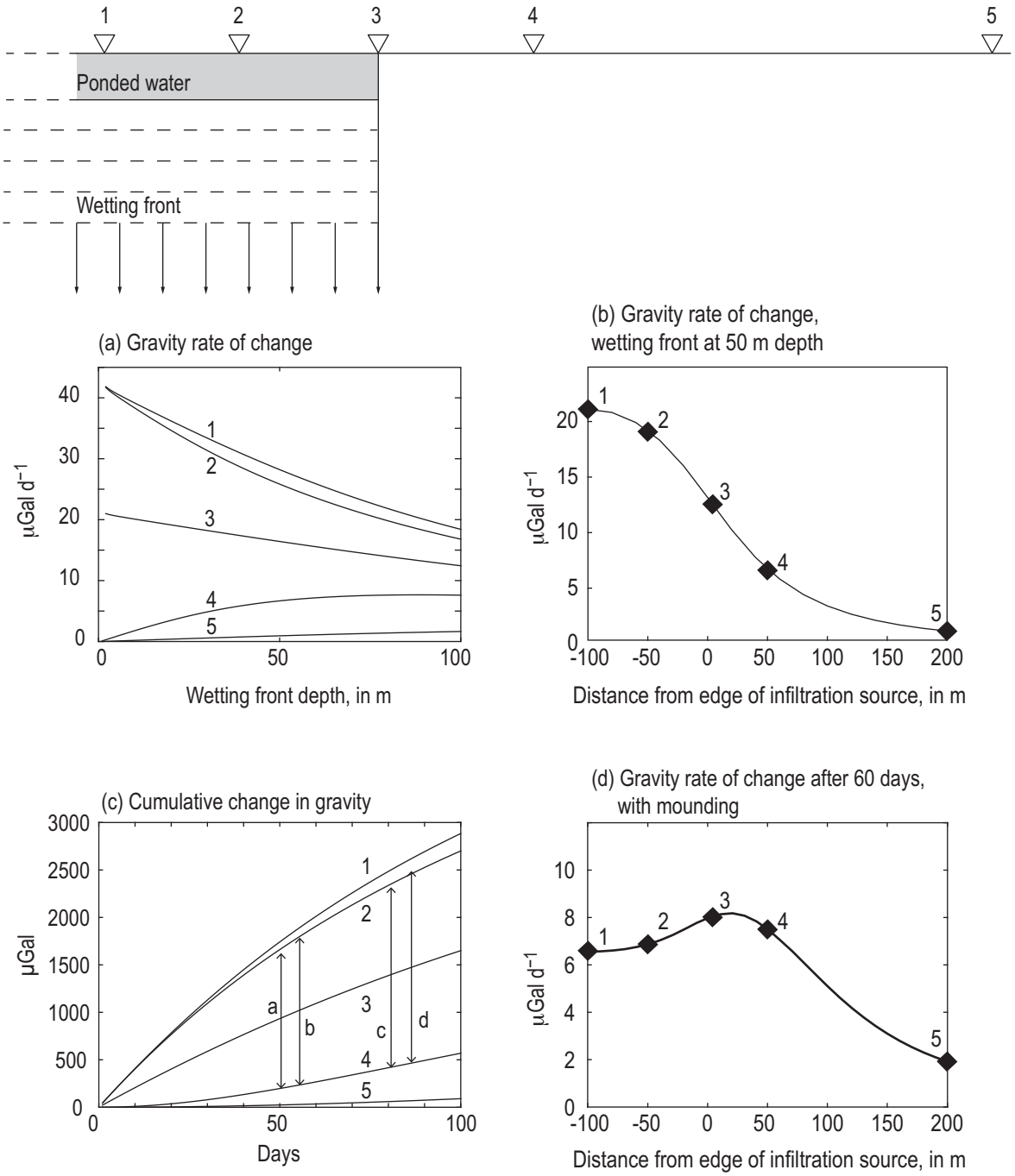

Figure 2. Schematic diagram showing the variation in gravity with distance from an infiltrating source. In this instance, the infiltration basin area is 200 m × 400 m, and stations are located −100 m, −50 m, 0 m, 50 m and 200 m from the basin edge (stations 1–5, respectively). Actual gravity change would be calculated by multiplying the values shown by porosity (i.e. the figures assume 100 per cent porosity). Throughout, numbered curves indicate data that would be observed at the respective numbered stations. In Fig. 2(c), 'a', 'b', 'c' and 'd' represent relative-gravity observations between the same two stations at four different times (see the text). Fig. 2(d) shows a hypothetical gravity rate of change for a more complex scenario with groundwater mounding and lateral flow.

infiltration process under a recharge basin into a deep, homogeneous vadose zone (Fig. 2). The rate of change of gravity (*dg/dt*) will be greater at stations closer to the centre of the infiltration source than at stations farther away (Figs 2a and b). During an episodic infiltration event, as more mass is added to the subsurface, gravity increases at all stations. But, because the distance to the centre of mass increases, *dg/dt* decreases over time at the nearest stations (Fig. 2a, stations 1, 2 and 3). Simultaneously, *dg/dt* increases at more distant stations (Fig. 2a, stations 4 and 5) as the angle between the horizontal and the centroid of the added water mass increases with time.

If only infiltration is considered (i.e. no groundwater mounding or lateral flow), we can approximate the gravity signal as a point source,

$$g_z = \frac{GMz}{(x^2 + z^2)^{\frac{3}{2}}} \tag{1}$$

where z is the depth of the centre of mass of added water from the surface, x is the horizontal distance at the surface between the gravimeter and vertical projection of the mass centroid, G is the gravitational constant and M is the added water mass. Even if the rate of advance of the wetting front is constant, dg/dt is a non-linear function of x and cannot be solved for directly in the network adjustment. In many real systems, at later times the downward movement of the mass centroid is accompanied by groundwater mounding and lateral groundwater flow. This reduces dg/dt near the source while causing dg/dt to be greater at stations further from the infiltration source (and mass centroid) than it would be if lateral flow did not occur. During drainage, the situation is more complicated. Lateral groundwater flow continues after infiltration stops, causing an increase in gravity as mass moves more directly beneath the gravity stations located further from the infiltration source. But, as water content decreases in the unsaturated zone, there is an accompanying decrease in density (and therefore gravity). In general, hydrologic processes lead to simultaneous increases and decreases in dg/dt with distance, which can result in complex distributions of dg/dt (Fig. 2d). For the field experiment presented here, absolute-gravity observations and numerical modelling indicate that the hydrologic processes described result in a quasi-linear relation of dg/dt versus distance, unlike the simulated response shown in Fig. 2(b). In Section 2.2.1, we detail network adjustment for cases that can be approximated by a linear relation. In Section 2.2.2, we consider the more general case, which requires the use of a process model for network adjustment.

2 METHODS

2.1 Network adjustment

Least-squares network adjustment of gravity data is used widely to combine absolute gravity, observed at single points, with relative-gravity differences observed between stations (Torge 1989). The absolute-gravity values establish the network datum in the same way that elevations at control benchmarks establish the datum in leveling surveys. Network adjustment combines redundant observations to determine a single best-fit gravity value at each station; in doing so, higher accuracy is achieved than if only single observations are made at each station. In addition, least-squares network adjustment provides information for evaluating the observation accuracy and uncertainty of the adjusted gravity values at each station.

For relative-gravity data, the observation equation can be written (Torge 2001)

$$\Delta g_{i,j} + v_{i,j} = g_j - g_i + \left[D\left(t_j\right) - D\left(t_i\right)\right] \tag{2}$$

where $\Delta g_{i,j}$ is the observed gravity difference between two successive stations i and j, $v_{i,j}$ is the residual error, g_i and g_j are the gravity values at stations i and j and $D(t_i)$ and $D(t_j)$ are the cumulative change in gravity at time i and time j, which can be modelled by a polynomial of degree a:

$$D\left(t\right) = \sum_{p=1}^{a} d_p (t - t_0)^p \tag{3}$$

$D(t)$ includes instrument drift and all other sources of gravity change that apply to the observations in the network adjustment.

Eq. (2), with a linear drift model (eq. 3), can be written in matrix form as

$$\begin{bmatrix} \Delta g_1 \\ \Delta g_2 \\ \vdots \\ \Delta g_n \\ Ag_1 \end{bmatrix} + \begin{bmatrix} v_1 \\ v_2 \\ \vdots \\ v_n \\ v_{Ag} \end{bmatrix} = \begin{bmatrix} -1 & 1 & 0 & \dots & 0 & 0 & t_{s2} - t_{s1} \\ 0 & -1 & 1 & \dots & 0 & 0 & t_{s2} - t_{s1} \\ \vdots & \vdots & \vdots & \dots & \vdots & \vdots & \vdots \\ 0 & 0 & 0 & \dots & -1 & 1 & t_{s2} - t_{s1} \\ 1 & 0 & 0 & \dots & 0 & 0 & 0 \end{bmatrix} \begin{bmatrix} g_1 \\ g_2 \\ \vdots \\ g_u \\ d \end{bmatrix} \tag{4}$$

or

$$\mathbf{L} + \mathbf{V} = \mathbf{AX} \tag{5}$$

If n is the number of observations and u is the number of unknowns, then $\mathbf{L}$ is an $n \times 1$ vector of observed gravity differences and absolute gravity observations and $\mathbf{V}$ is an $n \times 1$ vector of residuals. The matrix, $\mathbf{A}$, is the $n \times u$ design matrix with 1′s and -1′s to represent the 'from' and 'to' stations in each gravity difference. The last two columns of $\mathbf{A}$ are the parameters of the drift model and $\mathbf{X}$ is the $u \times 1$ vector of unknowns. In this case, the unknowns include both the gravity value at each station, as well as the polynomial coefficients in eq. (3) that describe the cumulative change in gravity with time.

If at least one constraint is included as a 'fixed' station (i.e. and absolute gravity or reference station) to overcome the rank defect of $\mathbf{A}$, eq. (4) can be solved using well-known least-squares methods to minimize $\mathbf{V}^{\mathrm{T}}\mathbf{PV}$, where $\mathbf{P}$ is the inverse of the covariance matrix that describes the accuracy of the observations. One or more absolute stations are represented by corresponding rows appended to the $\mathbf{L}$, $\mathbf{V}$ and $\mathbf{A}$ matrices (Hwang *et al.* 2002). The absolute-gravity values can be allowed to vary, or held constant by assigning a very low variance to the observation in the $\mathbf{P}$ matrix. In this example, the absolute-gravity values are allowed to vary, with a standard deviation of 5 μGal based on the estimated observation accuracy. Final gravity values for the absolute-gravity stations are determined from the network adjustment. Many additional network adjustment details, including solving the system of equations and outlier identification using the chi-squared test, are described in Torge (2001) and Hwang *et al.* (2002). For this study, the least-squares solution was implemented in Matlab (www.mathworks.com, last accessed 26 November 2015). Relevant code is available at http://go.usa.gov/375Gm (last accessed 26 November 2015).

In the most basic approach, $D(t)$ encompasses all gravity changes with time, including Earth tides and ocean loading, air pressure change, other geodetic effects and instrument drift. Hydrology-induced gravity changes are rarely, if ever, considered in the network adjustment. A more common approach removes Earth tides and ocean loading *a priori* using standard models, assumes air pressure change is negligible (in the case of consecutive relative-gravity stations observed within minutes to hours) or accurately measured, and ignores other geodetic effects such as polar motion or small elevation changes (Long & Kaufmann 2013). Then, $D(t)$ includes only instrument drift. In essentially all published network adjustments (e.g. Krieg 1981; Hwang *et al.* 2002; Touati *et al.* 2010), $D(t)$ is linear or piecewise-linear within a single measurement loop (a series of observations that start and finish at the same point). For this study, a non-linear *instrument* drift correction (not the correction

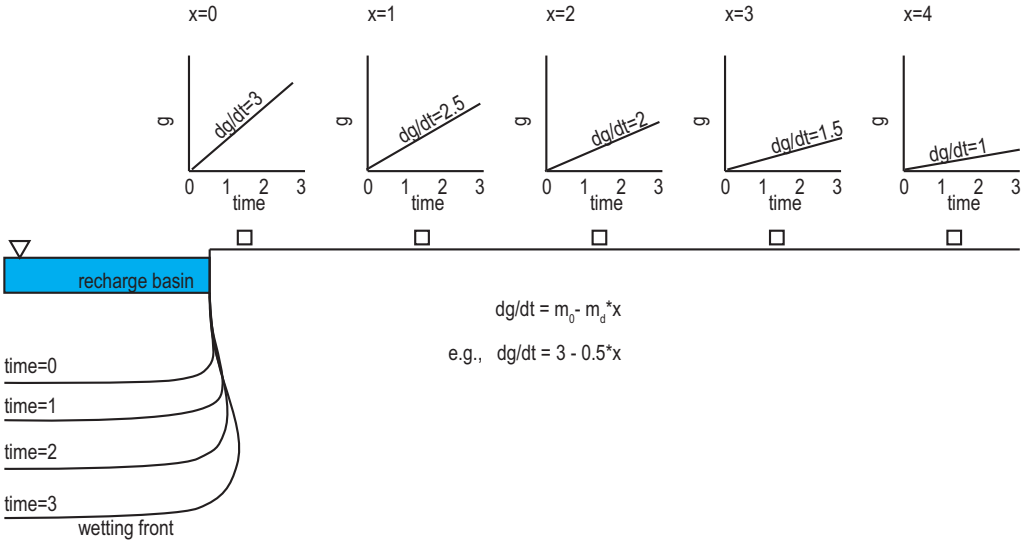

Figure 3. Schematic diagram of the linear *dg/dt*–distance model.

for hydrology-induced gravity change) is made possible by many small, overlapping loops, owing to the relatively small study area, short station spacing and high station repeat rate (Section 2.3.2). The drift correction is applied prior to and independently from the network adjustment, and as a result, $D(t)$ in eq. (2) represents only non-instrumental sources of gravity change with time.

In some instances, the observation eq. (2) includes a term to account for systematic error, including linear and periodic terms. The latter term accounts for circular screw error (an error introduced by the mechanical nature of the measuring screw found in Lacoste and Romberg gravimeters). Systematic error is not included in the adjustment in this example because absolute-gravity observations provide an independent source of gravimeter calibration. Circular error is not relevant because no screw adjustment is required given the small spatial area of this study, which is typical of many hydrology studies.

2.2 Modelling spatial variation in gravity change

To illustrate how a transient process can be accounted for during network adjustment, we consider a relative-gravity campaign with observations made at stations 3, 4 and 5 (Fig. 2) when the wetting front is at 50 m depth. Note that we consider here only vertical infiltration and not the more complicated infiltration, mounding and lateral flow that occurs in the field experiment. The relation between *dg/dt* and distance from the infiltration source (Fig. 2b) is modelled using the linear relation described in Section 2.2.1. The issue that we aim to address can be understood by examining a plot of cumulative gravity change (Fig. 2c). Consider the case for which the wetting front advances from 50 to 58 m depth during a field campaign (8 d, for this example where the wetting front advances 1 m d^{-1}). The gravity difference between stations 2 and 4 observed at the start of the campaign (labeled 'a' in Fig. 2c) will be smaller than the gravity difference observed between the same stations at the end of the campaign (labeled 'b' in Fig. 2c). The magnitude and sign of the change in the gravity difference depends on the time difference between the observations and *dg/dt* at both stations. Furthermore, later field campaigns may be subject to this effect with a different magnitude, even for the same two stations (e.g. Fig. 2c, times labeled 'c' and 'd'). Unless this effect can be quantified, this temporal change in gravity during a campaign will cause additional noise in a network-adjusted relative-gravity map.

2.2.1 *Spatial variation as a linear function of distance*

A simple approach to correct for the spatial variation in the rate of change of gravity over time (*dg/dt*) is to approximate it as a linear function of distance (x) from the edge of an infiltration basin (Fig. 3). The cumulative gravity change, D_h, at a station at distance x from the edge of the infiltration source after elapsed time Δt depends on *dg/dt* at that station, which is simulated as a linear function of x with intercept m_0 (gravity change at zero distance) and slope m_d:

$$D_h(x,t) = \left(\frac{dg}{dt}(x)\right)\Delta t = (m_0 - m_d x)\,\Delta t \tag{6}$$

With $\Delta t = t - t_0$, where t_0 is the start time of each campaign, substituting eq. (6) into eq. (2) and ignoring instrument drift (removed prior to the network adjustment) gives

$$\begin{aligned}\Delta g_{i,j} + v_{i,j} = g_j - g_i + \big[&\left(m_0 - m_d x_j\right)\left(t_j - t_0\right) \\ &- \left(m_0 - m_d x_i\right)\left(t_i - t_0\right)\big]\end{aligned} \tag{7}$$

or

$$\begin{aligned}\Delta g_{i,j} + v_{i,j} = g_j - g_i + m_0(t_j - t_i) \\ - m_d\left[x_j\left(t_j - t_0\right) - x_i\left(t_i - t_0\right)\right]\end{aligned} \tag{8}$$

x and t are known for each observation; $\Delta g_{i,j}$ is observed using a relative gravimeter, and g_i, g_j, m_0 and m_d are coefficients to be identified as part of the least-squares solution. The parameters $(t_j - t_i)$ and $(x_j t_j - x_i t_i)$ are included as additional columns in the design matrix $\mathbf{A}$ and m_0 and m_d are included in the solution vector $\mathbf{X}$ (eq. 5).

Previous studies have generally treated the fixed gravity values at the absolute gravity stations in the network as known values. In that case, the elapsed time in eq. (6) refers to time since the beginning of the relative-gravity campaign. In extreme cases, such as the field experiment presented here, gravity at the fixed stations will change between the time of absolute-gravity data collection and the start of the campaign. In that case, the time of the relative-gravity observations must be specified relative to the time of the absolute-gravity observations.

2.2.2 Numerical model

An alternative to the linear approximation of the variation of dg/dt with distance is to estimate directly the change in gravity at each station at each observation time using a numerical groundwater model. This is an example of coupled hydrogeophysical inversion (Ferré *et al.* 2009). As employed here, this method couples the solutions of a geophysical instrument model (i.e. the processing steps required to convert sensor readings into measured quantities, in this case the network adjustment), a petrophysical model (i.e. that converts measured quantities into hydrologically relevant parameters) and the hydrologic model itself. In this case, the hydrologic model is also the petrophysical model, because it defines the 3-D distribution of mass change that allows gravity change to be related to water-storage change. If the ultimate (and only) goal is to calibrate the hydrologic model, the coupled inversion could avoid network adjustment altogether if the observed gravity differences were used as calibration data directly. Redundant measurements could still be made, but they would be used in the non-linear parameter-search/estimation process undertaken during calibration of the hydrologic model. This approach forgoes the well-established uncertainty estimates that least squares provides. Another potential drawback of using gravity differences for calibration directly is that maps of gravity at a single epoch (or change in gravity between epochs) would have to be derived from the output of the hydrologic model, rather than from the data directly. In this case, the gravity maps would include error due to uncertainties in hydrologic model structure and parametrization.

To simulate more complicated spatial variation in the rate of change of gravity than can be accommodated by the linear model, a single-layer Modflow–NWT numerical groundwater model was constructed (Niswonger *et al.* 2011). Infiltration below the recharge basins was modelled using the unsaturated-zone flow (UZF) package (Niswonger *et al.* 2006), which implements the Brooks–Corey infiltration model (Brooks & Corey 1964) and a sequence of kinematic waves to represent water content profiles. A 4000 × 2700 m model domain, centred on the three recharge basins, was discretized into 25 m cells. The actual durations and rates of infiltration, as observed from field data, were simulated at each basin. The model was run in transient mode for 490 d, the duration of the period during which continuous gravity data were collected. The time periods relevant to the relative-gravity campaigns are from days 396–404, 431–434 and 458–461; for this example, the initial 336 d period prior to the last infiltration cycle can be considered a model initialization period.

In the UZF Modflow package, the change in water content in the unsaturated zone, and therefore the change in density and gravitational attraction, is determined by the ratio of the infiltration flux, q_{in}, to saturated hydraulic conductivity, K_{s}; the Brooks–Corey exponent, ε; the specific yield, S_{y} and the residual water content, θ_{r} (Niswonger *et al.* 2006):

$$\theta = \left(\frac{q_{in}}{K_s}\right)^{1/\epsilon}(S_y) + \theta_r \quad 0 < q_{in} \leq K_s \tag{9}$$

The UZF package assumes the downward flux is equal to the unsaturated hydraulic conductivity and ignores capillarity forces. Specific yield is the difference between the saturated and residual water content. Because gravity change is linear with density change, model-predicted gravity is sensitive only to the change in water content rather than the absolute value of water content. We chose to keep the saturated water content constant and to vary θ_{r} to achieve a range of S_{y} values. The upper limit for infiltration flux was set to K_{s} to avoid ponding and overland flow.

The change in gravity simulated by the model was calculated at each gravimeter position for the saturated and unsaturated parts of each cell of the groundwater model. Groundwater storage change was considered only at the water table and assumed zero in the saturated part of the aquifer (i.e. zero compressibility). For model cells where the UZF package was active, the vertical column between the land surface and the water table was discretized into 40 rectangular prisms and the change in volumetric water content in each prism used as the density change in the gravity model. Gravity was calculated by the prism (Nagy 1966), MacMillan (1958), or point-mass formulae depending on the relation between the distance from the gravimeter to centre-of-mass change and the dimensions of the element (Leirião *et al.* 2009).

For the purpose of the network adjustment, the groundwater model is used only to simulate the redistribution of water mass from the recharge basin into the subsurface, so that the gravity rate of change can be estimated at each station. A simple gradient-based parameter search was used to estimate a best-fit set of parameters, based on the mean-square error between simulated and observed gravity at the seven locations where absolute-gravity data were collected (Fig. 1). No other data were used for calibration. At the two locations with continuous gravity data, RB206 and RB207, the 15-month record was sampled at equal intervals 20 and 15 times, respectively. There are 10 or 11 observations at each of the remaining stations. All observations are weighted equally, but by including more observations from the locations with continuous data the inversion implicitly gives greater weight to this higher quality data. The MATLAB function fmincon was used in 'multistart' parallel processing mode, with 20 initial starting points distributed evenly in the parameter space. The model parameters and bounds were K_s (0.2 – 10), S_y (0.15 – 0.4), vertical K_s in the unsaturated zone (0.2 - 0.6) and Brooks–Corey exponent (1 - 12). K_{s} bounds were selected based on observed infiltration rates; the latter two parameter bounds were selected to encompass the range of physically likely values. Although the single-layer Modflow model only simulates horizontal groundwater flow, the UZF package allows for a different hydraulic conductivity value in the unsaturated zone.

2.3 Relative-gravity data

We examine the effects of correcting for hydrologic processes in two ways. First, we develop a synthetic data set that mimics the observations acquired in the field. We construct this synthetic case with known values for m_d and m_0 (representative of the values observed in the data). Varying levels of random noise is added to the synthetic data and the network adjustment performed. This allows us to quantify and understand the effects of ignoring hydrologic processes in interpreting gravity data. Then, we interpret the data collected in the field, applying our proposed network adjustment with consideration of hydrologic effects.

2.3.1 Simulated data

Every relative-gravity field study is constrained by the time available, traveltime between stations and station accessibility. In addition, seismic activity or instrumentation issues can make it difficult to follow exactly the prescribed survey schedules and observations may need to be collected as conditions allow. Therefore, it is difficult to make broad conclusions applicable to every possible network.

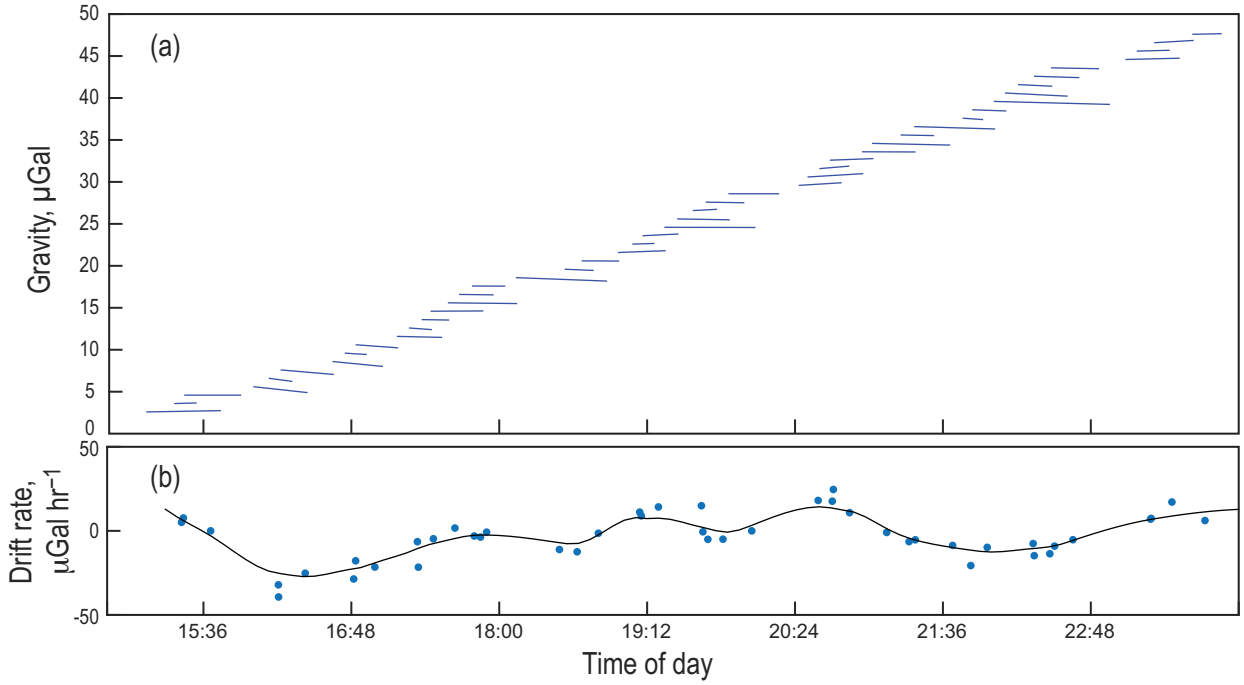

Figure 4. Selection of field data showing instrument-drift model. In panel (a), the two ends of each line show the observed gravity values at a station where a repeat observation was made, with intervening occupations at other stations in between. Therefore, each line, and the corresponding drift rate in panel (b), represents a closed loop. The slope of each line is the drift rate (station pairs are plotted in observation order from bottom to top; the vertical offset between station pairs is arbitrary). In panel (b), each marker shows the drift rate plotted at the time midway between the two station occupations. The solid line shows a LOWESS smoothing model fit to the data. This modelled drift is independently removed from the data prior to the network adjustment.

Instead, the survey order of relative-gravity observations collected during the field experiment in Section 2.3.2 is used to form the design matrix **A** (eq. 4). A series of gravity differences was simulated between successive stations using the station distances and observation times to match the field data, the model defined by eq. (8) and representative values for m_d and m_0. The field-observed gravity differences are not used in the simulated data set. A Monte Carlo simulation was used with the network adjustment to estimate the statistics of the observation residuals and station residuals. To do so, 5000 samples were generated with varying levels of normally distributed random noise of known standard deviation added to the true values.

2.3.2 Field data

Relative-gravity data were collected on a network of 72 stations, including seven colocated absolute gravity stations. Earth tide and ocean loading corrections were calculated using local tide parameters derived from continuous gravity data (Kennedy *et al.* 2014). During each campaign, relative-gravity stations were generally observed in the pattern A-B-C-B-A-C-D-E-D-C-E-A (letters refer to station order), which results in a data set with about three times the minimum number of gravity differences required to assign a gravity value at each station during network adjustment; these redundant measurements reduce uncertainty. Approximately 4–8 repeat measurements were made each hour (Fig. 4). Each station repeat [i.e. for the A-B-C-B-A-C order, occupations 1 and 5 (A-A), 2 and 4, (B-B) and 3 and 6 (C-C)] represents a closed loop from which drift can be estimated. The drift rate indicated by the lines in Fig. 4a are not based on a single occupation at a single station but rather on repeat occupations with other stations in between (traditionally referred to as a loop). This differs from traditional adjustment in that the drift is modelled as a continuous function of time from many, overlapping loops. The traditional approach would be to divide observations into single, discrete loops (or other subsets), each with its own drift-model parameters.

The high repeat-occupation rate is possible due to the short station spacing and traveltimes, and allows a non-linear drift curve to be fitted to the individual drift estimates using locally weighted smoothing (LOWESS) (Fig. 4b). The general pattern for the survey shown in Fig. 4b is that of steadily increasing drift during the day; this behaviour is typical of the Burris gravimeter used in the study (drift curves for all data in the study are at http://go.usa.gov/375Gm). The cumulative drift at any station observation is calculated by integrating the region under the modelled drift curve (Fig. 4b). But, because only relative-gravity differences between subsequent stations are used in the network adjustment, only the 'differential drift' between the two stations comprising the difference applies. Because the traveltime between stations is generally short for the study area (2–5 min), the drift correction is relatively small. The calculated differential drift is removed from the gravity differences prior to adjustment. This approach treats instrument drift as a continuous function of time, rather than the standard approach of applying a drift correction to discrete 'loops' using parameters included in the network adjustment. It is potentially a more flexible approach than including drift as a linear term in the network adjustment because drift can be non-linear, even over a few hours. Also, because the instrumental-drift frequencies overlap with those of the gravity change caused by hydrology, removing the former as a processing step improves the ability of the least-squares adjustment to resolve the latter.

Absolute gravity was observed at seven stations using an A-10 absolute gravimeter (Schmerge & Francis 2006; Schmerge *et al.*

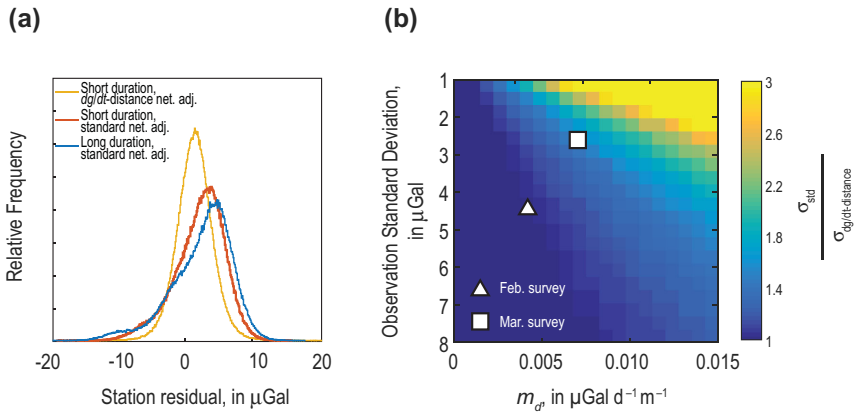

Figure 5. Plots showing the error introduced by not including the spatial variation in *dg/dt* in the network adjustment. (a) Histogram showing the residuals between simulated (known) gravity values at each station and network-adjusted results and (b) ratio of the standard deviation of the residuals from the standard adjustment (one that does not include the spatial variation of *dg/dt* in the adjustment) to the standard deviation of the residuals from the *dg/dt* adjustment model. Warmer shading indicates the increasing effect of including spatial variation in *dg/dt* in the network adjustment. Markers show the least-squares-predicted m_d value for each field campaign (net adj., network adjustment).

2012). Absolute gravity observations are used to provide the datum associated with each relative-gravity survey, and to estimate *dg/dt* during each campaign in order to define the *dg/dt*–distance relation. Based on prior experience (Schmerge & Francis 2006) and comparison with the continuous gravity record, the estimated uncertainty (standard deviation) of the A-10 observations is 5 µGal at this site. The uncertainty of the *dg/dt* estimate was calculated by summing in quadrature the uncertainty of the two observations comprising the *dg* estimate, divided by the length of time between the observations. Three of the eight absolute-gravity stations, including the continuous sites, were inside small control buildings; the remaining sites were on concrete monitoring-well pads approximately 1 m thick. Absolute-gravity observations were made at each station before and after each of the three campaigns for a total of six rounds of observations. Continuous data were recorded at two sites adjacent to the recharge basins (colocated with absolute-gravity observations) using a combination of iGrav superconducting gravimeters and gPhone gravimeters (GWR, Instruments, Inc. and Micro-g Lacoste, Inc.). No significant rainfall occurred during the experiment.

3 RESULTS

3.1 Linear *dg/dt*–distance model, simulated data

The simulated gravity data described in Section 2.3.1 and the linear model are used to investigate the importance of including *dg/dt* in the network adjustment. Typically, the time between t_i and t_j (eq. 8) will be short relative to the total time of a campaign, and as a result m_0 has low leverage and influence in the network adjustment (similarly, m_d would be poorly identified if the distance x was nearly the same for all stations). This result was verified by testing a range of m_0 values, which caused no meaningful difference in the following results.

Our analyses are based on residuals between the known (simulated) gravity values at each station and the network-adjusted values calculated for each of the 5000 Monte Carlo simulations ($m_d = 0.007$ µGal d^{-1} m^{-1}, $m_0 = -2.5$ µGal d^{-1}, measurement noise = 3 µGal standard deviation). Composite probability distribution functions were calculated by combining the residuals, between the true gravity value at each station and the network-adjusted value, for all simulations. When there is no spatial variation in *dg/dt*, or when spatial variation is correctly modelled in the adjustment using eq. (7), the residuals are effectively identical in both cases and approximately Gaussian (Fig. 5a, orange series, *dg/dt*–distance network adjustment). The variance of the residuals in this case is determined by the observation variance and is not affected by the campaign duration. The largest absolute residual is about 10 µGal. If there is spatial variation in *dg/dt* that is not included in the network adjustment (Fig. 5a, red and blue series, standard network adjustment), the variance of the residuals and the skew both increase. In this example, the distribution has negative skew, as observations made later in the campaign (on the left side of the distribution) have increasingly greater error; if m_d had opposite sign, the skew would be positive. The campaign duration is also important; for a longer campaign, the effect of the *dg/dt*–distance relation is increasingly important; a survey that took twice as long as the March campaign would have even greater skew (Fig. 5a, blue series, long-duration standard network adjustment).

We extended our analysis of the effects of the spatial variation in the rate of change of gravity with time on the overall survey error for a range of m_d values and measurement noise. The latter is important because m_d may be hidden by the signal-to-noise ratio for overly uncertain observations. A metric was defined as

$$\varepsilon = \frac{\sigma_{\text{std}}}{\sigma_{dg/dt}} \tag{10}$$

to provide an estimate of the additional error introduced in the adjusted gravity values when the change in gravity during a campaign is not included in the adjustment. In eq. (10), σ_{std} is the standard deviation of the residuals for the standard network adjustment and $\sigma_{dg/dt}$ is the standard deviation of the residuals (for the same input data) when the linear *dg/dt*–distance model (eq. 8) is included in the adjustment. If observation uncertainty is low, ε is higher, indicating that accounting for transient hydrologic processes is more important in the adjustment (yellow regions on Fig. 5b). On the other hand, the blue regions of Fig. 5(b), where $\varepsilon = 1$, represent cases for which observation uncertainty is high and (or) m_d is low, so little additional error is introduced by performing the standard network adjustment. Considering the February campaign, for the observed value of m_d (–0.0043 µGal d^{-1} m^{-1}, Fig. 6) and an estimated observation accuracy of 4.3 µGal (the *a posteriori* estimate from the network adjustment), ε is near 1 (Fig. 5b). This suggests that consideration of hydrologic change during the campaign is not critical

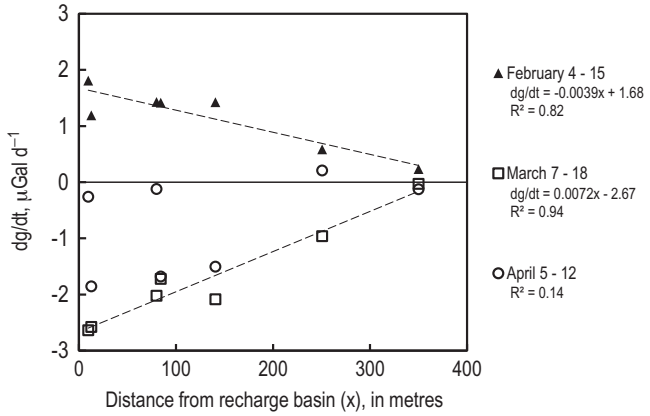

Figure 6. Observed gravity rate of change (A-10 absolute-gravimeter data) versus distance from the edge of a recharge basin. Lines are best-fit linear models determined by the network adjustment solution. Dates are those of the absolute-gravity observations, which bracket the relative-gravity observations during each campaign. The average standard deviation of the observed *dg/dt* (i.e. the vertical error bars) for the February, March and April surveys is 0.32, 0.64 and 0.83 µGal d^{-1}, respectively.

for the February campaign. In contrast, for the March field campaign, for the observed value of m_d (0.0072 µGal d^{-1} m^{-1}, Fig. 6) and an estimated observation accuracy of 2.5 µGal, ε is about 1.5 (Fig. 5b). This implies the March campaign would have about 50 per cent greater error if the variation in *dg/dt* with distance was not included in the network adjustment.

3.2 Linear *dg/dt*–distance model, observed data

Absolute-gravity data provide an estimate of the expected m_d values identified by the network adjustment. During the February and March campaigns, *dg/dt* varies approximately linearly with distance (Fig. 6). In February, when there is ponded water in the basins, gravity increases fastest at stations close to the basins and *dg/dt* decreases with distance (m_d is negative). In March, after the basins have dried, gravity is decreasing most rapidly at stations close to the basins, and *dg/dt* increases (approaches zero) with distance (m_d is positive). In April, the relation is not first-order linear; two stations at intermediate distance have the most-negative *dg/dt*, whereas the other stations are near zero. This non-linearity as compared to the earlier surveys likely results from two factors. First, at the time of the April survey, about two months after infiltration has stopped, the groundwater mound has decreased substantially and the stations nearest the basins (RB206 and RB207) are no longer declining rapidly. Second, the two stations with the most-negative *dg/dt* (SA011A and SA015A) are both east of the basins and the difference in *dg/dt* may result from preferential flow and storage in the east–west direction. Therefore, the absolute gravity data would

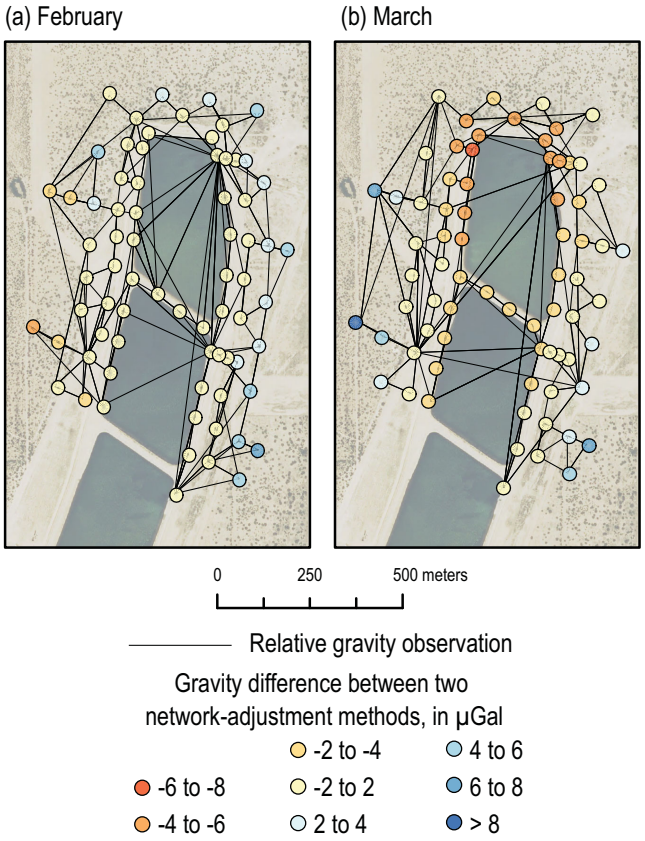

Figure 7. The difference in adjusted gravity values between the standard adjustment (one that does not include the spatial variation of *dg/dt* in the adjustment) and the adjustment that includes the linear *dg/dt*–distance model. Positive values indicate the standard adjustment-predicted gravity value is higher than the *dg/dt*–distance adjustment-predicted gravity value.

support using a linear model for adjustment in February and March, but not for the April campaign.

The *dg/dt*–distance network adjustment predicts m_d values that are similar to the observed values in both sign and magnitude (Table 1). The predicted m_d value for the February survey is more negative than the observed value. This may indicate that the *dg/dt*–distance relation is more non-linear than predicted by the absolute gravity data (Fig. 6). The predicted m_0 values (not shown) are poorly constrained by the network adjustment, but m_0 was shown to not have a large influence on the predicted m_d values nor on the adjusted gravity values (code available at http://go.usa.gov/375Gm).

The difference in the network-adjusted gravity value (Δg_{nw}) at each station between the two adjustments—the one that includes spatial variation and the one that does not—shows the effect of the linear *dg/dt*–distance model (Fig. 7). Each campaign began with

Table 1. Observed and network-adjustment-predicted m_d and mean observation residual from the network adjustment.

Campaign	Dates of relative-gravity observations	Observed m_d from absolute *g* data, µGal d^{-1} m^{-1}	Predicted m_d from network adjustment, µGal d^{-1} m^{-1}	*A posteriori* observation standard deviation from network adjustment, µGal
February	2013 February 5 to 2013 February 8, February 13, February 25	−0.0039	−0.0086 ± 0.0022	4.3
March	2013 March 12 to 2013 March 15	0.0072	0.0065 ± 0.0036	2.5

observations in the southeast part of the network and progressed in a generally counter-clockwise direction, with occasional ties to (primarily) absolute-gravity stations in other parts of the network. The February campaign (Fig. 7a) shows the effect of this observation pattern: at stations observed early, the standard network adjustment overestimates gravity (in blue) and at stations observed late in the campaign the standard network adjustment underestimates gravity (in red). The difference between the two methods is greater for the March campaign (Fig. 7b). In part this is because the reference time for the absolute gravity measurements for the February campaign (February 11) is midway through the period when relative-gravity data were collected. For the March campaign, the reference time for absolute gravity measurements is prior to the start of the campaign, March 7. This highlights the importance of including the spatial variation of *dg*/*dt* in the network adjustment when time elapses between absolute-gravity data collection at the stations that are fixed in the network adjustment and relative-gravity data collection.

3.3 Numerical model

For maximum flexibility in the network adjustment, a numerical groundwater model can be substituted for the linear *dg/dt*–distance model. For our field experiment, there are two main reasons that the model would not be linear: the recharge basins are elongated in a north–south direction, but stations are located on three sides; and, there are nearby public-supply wells to the east and south but not to the north or west. Using the numerical model, the model-simulated gravity change during a campaign is removed prior to, rather than as part of the network adjustment. For the sole purpose of estimating gravity change during a campaign, the groundwater model needs to accurately represent the spatial variation in gravity over the short duration of each relative-gravity campaign.

A single optimum parameter set for the Modflow model was found by minimizing the mean-square error between observed and predicted gravity at seven stations (K_s = 5.7 m d^{-1}; S_y = 0.30; vertical K_s in the unsaturated zone = 0.43 m d^{-1}; Brooks–Corey exponent = 7.2). The model replicates the observed gravity change reasonably well (Fig. 8). Mean absolute error is 15.5 μGal, which is larger than the estimated observation error of 5 μGal. Model error is attributed to (1) absence of aquifer parameter heterogeneity in the model, (2) simplification of the infiltration and drainage processes

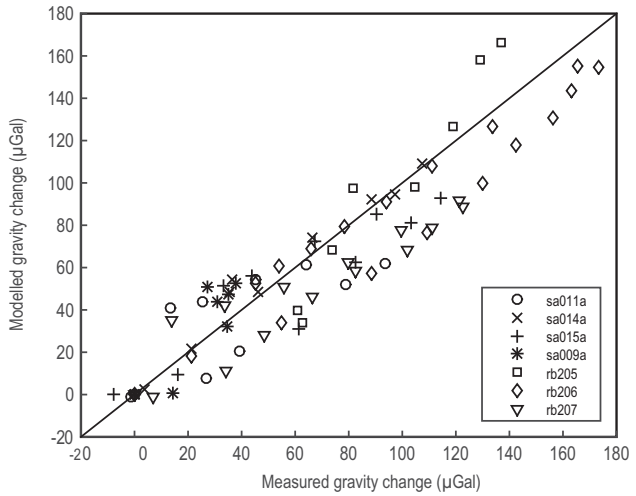

Figure 8. Calibration gravity data and simulated values from the numerical groundwater-flow model. Observed data are from stations where absolute-gravity data were collected.

in the UZF package and (3) simplification of the model domain, including simulating only three of the nine infiltration basins and excluding more distant pumping wells. A more extensive modelling effort is beyond the scope of this paper. Rather, we show this analysis as an example of an application where the primary product is a gravity (or gravity-change) map. In this case, a model that simulates the spatial variation of gravity may suffice, even if the accuracy of model parameters or predictive capacity is limited.

The adjusted relative-gravity snapshots for each measurement time are shown in Fig. 9. The left column shows the results interpreted using the standard adjustment, the middle column shows the results with the modelled *dg*/*dt* removed and the right column shows the differences between these two interpretations. From a qualitative standpoint, maps showing gravity change between campaigns are largely similar, regardless of whether spatial variation in *dg/dt* is included in the network adjustment (Fig. 9). The gravity-change maps can be interpreted directly. Notably, the change in gravity is not symmetric about the apparent centre of mass based on the extent of the basins. Instead, between February and April a large proportion of the gravity decrease is focused on the eastern edge of the basins, thus indicating where drainage was most efficient. Meanwhile, the greatest increase in gravity, and therefore groundwater storage (caused by lateral flow of recharged water) occurs to the west of the basins. Because all three basins shown in Fig. 9 were flooded and dried on the same cycle, one would expect an elongated N-S region of gravity change, centred E-W within the basins. The observed spatial variation in gravity change likely indicates spatial heterogeneity of infiltration and pumpage from well AV019A and other nearby wells. In fact, infiltration rates based on observed inflow rates in RB205 and RB206 (the two basins to the south) are 20–30 per cent higher than in RB207.

The difference between the two methods (the standard network adjustment that does not account for the *dg*/*dt*–distance relation, versus using the numerical groundwater model to correct for the change at each station) with respect to the gravity change between campaigns, ranges from −5.5 to 4.7 μGal (Fig. 9, right; Table 2). Brighter colours in the right column of Fig. 9 show the stations where the inclusion of the simulated gravity from the model has the greatest effect. Positive values indicate that the estimated gravity change predicted using the groundwater model-corrected values is higher than the change estimated using the standard network adjustment. For the February–March difference (Fig. 9a), the standard network adjustment results in an estimated gravity change that is smaller than using the groundwater-model corrected gravity differences in the network adjustment; the mean difference is 0.4 μGal (Table 2). The large positive differences to the west are caused by observing these stations late in the February campaign, up to 9 d after the start. The two stations with the largest negative difference (in blue, right column of Fig. 9a), immediately west of the centre basin, are separated from the nearby stations to the west by a fence. These two stations were observed on different days than the stations to the west, and are not directly connected in the survey network (Fig. 7), thus showing the effect of the network design on the adjusted results. For the March–April gravity difference (Fig. 9b), the effect of not including spatial variation is to shift the centre-of-mass change further west (the blue-shaded region in the right-hand panel becomes ‘cooler’ in the central panel when spatial variation is considered).

Similar to the pattern seen with the single-campaign gravity fields (Fig. 7), the difference between the standard adjustment and the groundwater-model-corrected approach reflects the order in which observations are collected. To demonstrate, the magnitude of the estimated change in gravity between campaigns (February to March

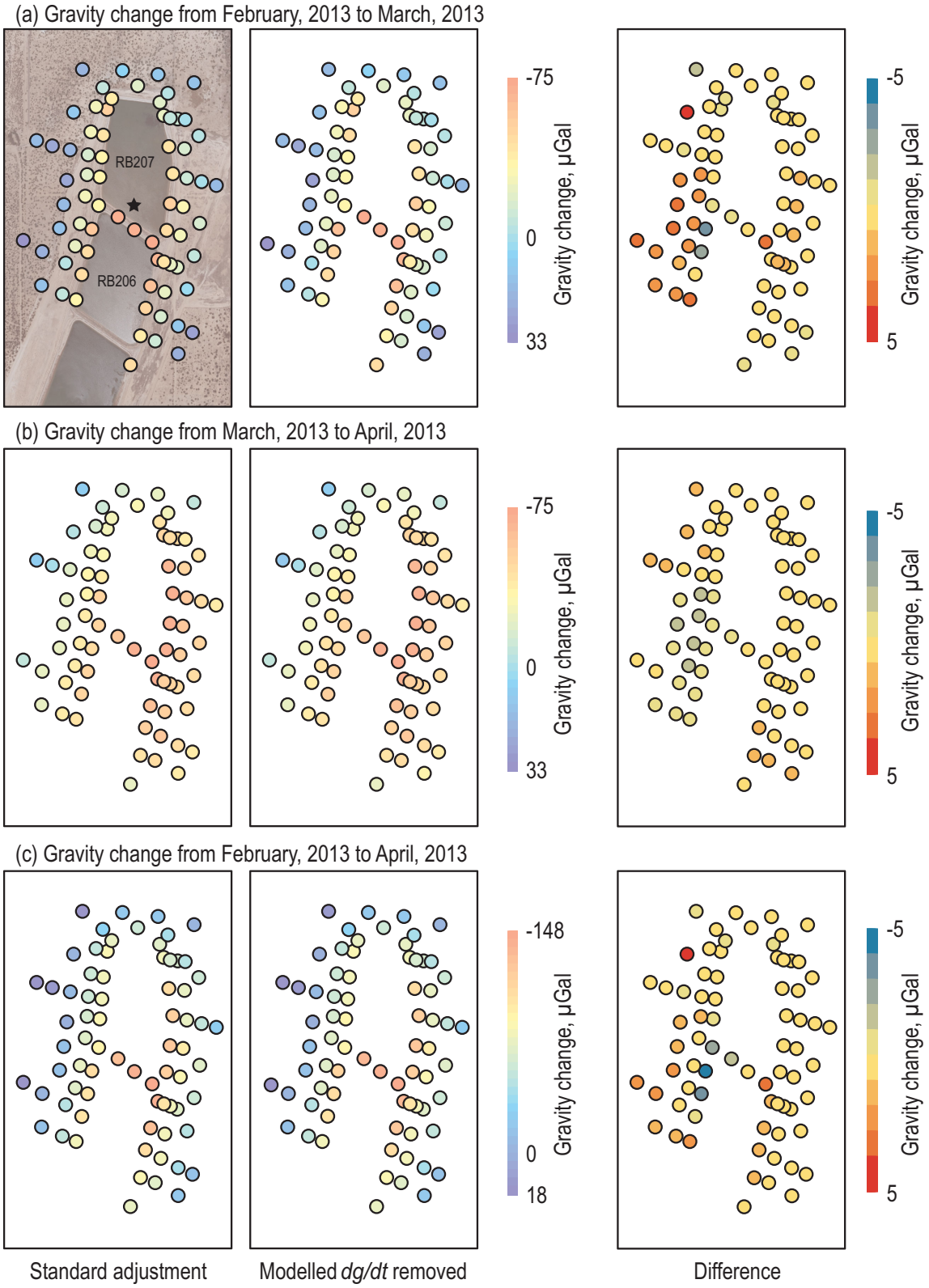

Figure 9. Maps showing the change in gravity between relative-gravity campaigns using alternately a standard network adjustment (left-hand panels) and a groundwater-flow model to account for the spatial variation in *dg* during a campaign (centre panels). The difference between the methods is shown in the right-hand panels. Standard adjustment refers to one that does not include spatial variation in *dg/dt* in the adjustment. In the right-hand panels, positive values indicate that the estimated gravity change predicted using the groundwater-model-corrected values is higher than the change estimated using the standard network adjustment. The star in the top-left-hand panel shows the position from which the azimuth shown in Fig. 10 is calculated.

Table 2. Statistics of the difference, in μGal, between the standard network adjustment and the groundwater-model-corrected data, with respect to the estimated change in gravity between three relative-gravity campaigns. Data that the statistics describe are shown in map view in the right-hand panels of Fig. 9, and in Fig. 10.

	February to March	March to April	February to April
Minimum	−4.3	−2.0	−5.5
Maximum	3.8	0.9	4.7
Mean	0.4	−0.3	0.1
Mean absolute	0.9	0.6	0.8

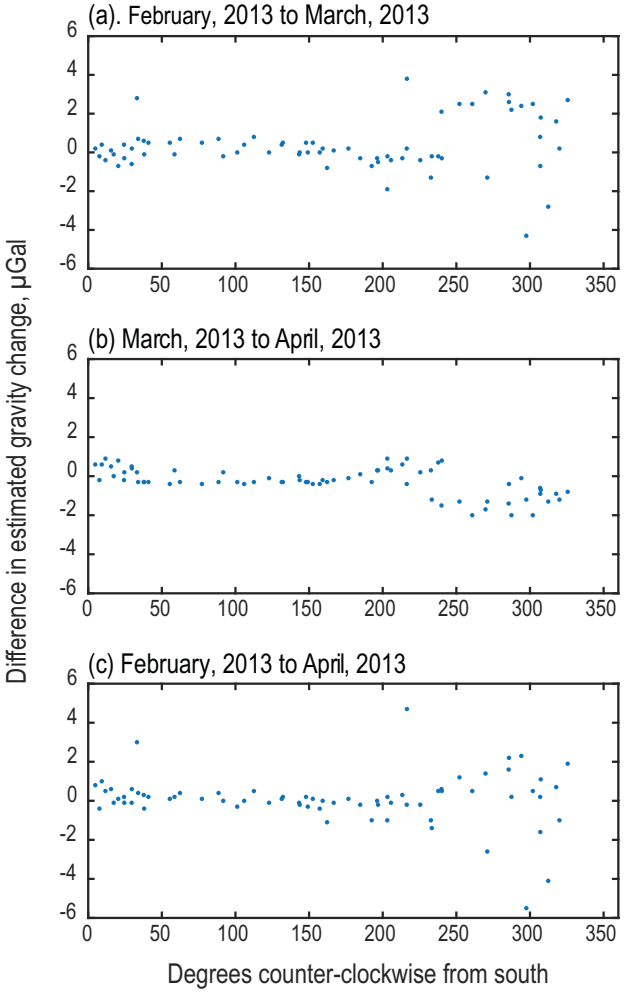

Figure 10. Scatterplots showing the difference between the standard network adjustment and the groundwater-model-corrected data, with respect to the estimated change in gravity between three relative-gravity campaigns (February to March and March to April). The same data are shown in map view in the right-hand panels of Fig. 9. The increasing difference with angle from south reflects the generally counter-clockwise order (starting from the south) of the relative-gravity surveys.

and March to April) is plotted in Fig. 10 as a function of azimuth from a central point in the basins (marked by a star in Fig. 9a, left). Because surveys during all three campaigns generally progressed from the southeast counter-clockwise to the southwest, the difference in the estimated gravity change accumulates as the survey progresses (represented by the increasing angle in Fig. 10). For the field study presented, the most significant error arises during the latter third of the survey; these are observations made primarily during the latter part of day 3, and later, during the respective campaign.

Error introduced by using the standard network adjustment instead of accounting for spatial variation adds to the complexity of calibrating an accurate hydrologic model. Furthermore, a model that did fit the results from the standard network adjustment would lead to misunderstanding of the actual hydrologic processes occurring at the site, including the direction of groundwater flow and accumulation of groundwater storage. Ultimately, this demonstrates the advantage of coupled hydrogeophysical inversion: understanding of spatial and temporal relations, described by a hydrologic model, allows for improved interpretation of geophysical data, and consequently, improved hydrologic insight.

4 CONCLUSIONS

There is increasing interest in the use of geophysical data for hydrologic investigations (Binley *et al.* 2015). Efficient extraction of hydrologically relevant information from geophysical data requires careful consideration of the interactions of geophysical observation and hydrologic process. In this study, we show that these considerations extend even to fundamental processing of geophysical data. Specifically, processing relative-gravity data requires many steps—removing Earth tides and ocean loading, averaging several readings at each station, correcting for instrumental drift, tares and systematic error, measuring absolute gravity and adjusting the network to a common datum, differencing between campaigns—and each represents a possible source of error. By considering the change in gravity during the field campaign as part of the network adjustment, this additional error source is minimized, which may ultimately enable observations of otherwise obscured hydrologic processes. We present a conceptual approach to consider transient hydrologic processes during gravity processing, a simple example of coupled hydrogeophysical inversion. Generally, coupled inversion requires that geophysical data are interpreted in the context of a hydrologic model, rather than as a prior independent step. In this case, the hydrologic model informs the network adjustment, which can be viewed as the instrument response model (i.e. the model required to transform observed quantities to useful values).

Our proposed approach is based on the observation that the rate of change of gravity data with time, dg/dt, varies spatially and temporally in the presence of overlapping transient hydrologic processes. In some cases, a linear dependence of dg/dt on spatial location can be justified. This simplifies network adjustment and removes the need for more rigorous coupled hydrogeophysical inversion. For the field study presented, an approximately linear relation is observed in the A-10 absolute-gravity observations and is supported by the groundwater model. Two other common hydrologic scenarios may also lend themselves to relatively simple models (but not necessarily first-order linear) to simulate the distance–dg/dt relation: a survey around a pumping or injection well in which radial symmetry is assumed and infiltration beneath an ephemeral stream channel, where dg/dt might be linear with distance from the stream channel due to the combined effects of infiltration and groundwater mounding. For smaller rates of gravity change and larger study areas, however, the gravity rate of change is unlikely to be linear and a numerical model is warranted. For studies covering large areas, the increased traveltime between stations and fewer repeat occupations result in greater uncertainty in the drift correction, and therefore in the relative-gravity differences. In these cases, a low signal-to-noise ratio may reduce or eliminate the usefulness of the gravity rate-of-change correction.

The general approach of simulating gravity change that occurs during a relative-gravity field campaign applies to other fields beyond groundwater hydrology. For a field campaign where significant rainfall occurred between surveys, a watershed rainfall-runoff model could simulate the gravity changes in water storage and redistribution. For volcano studies, a process model of magma-chamber deformation could be used. The approach could also be extended to iterative model calibration. In this approach, a starting model is developed, the network adjustment for each campaign performed and the gravity differences between campaigns are used to calibrate the model. Each successive model improvement results in a better simulation of changes in the gravity field and therefore more accurate network adjustment. The network adjustment could even be avoided altogether, and observed gravity differences could be predicted directly as an example of fully coupled hydrogeophysical inversion.

The primary factor that determines the importance of including the change in gravity during a campaign in the network adjustment is the rate of change relative to the duration of the campaign. For the field example presented, each relative-gravity campaign was carried out rapidly. However, campaigns that take place over several weeks are not uncommon (e.g. Chapman *et al.* 2008; Sugihara & Ishido 2008; Kennedy 2015). Another influencing factor is the spatial extent of rapid gravity change relative to the extent of the network; if only a few stations are expected to change relative to the others during a campaign, applying the linear model to all stations may be inappropriate. Finally, the precision of the observations is important: if relative-gravity observations approach μGal accuracy, it is more likely that consideration of transient processes during a campaign, hydrologic or otherwise, will be required.

Ultimately, the approach presented here is only required due to the limitations of present-day gravimeters. If very accurate (sub-μGal) observations could be made very quickly or even continuously, at a large number of stations, at reasonable cost, there would be no need for network adjustment, much less the accommodation of the spatially variable gravity rate of change. In this regard, improvements in gravity field instruments will continue to affect gravity survey designs and analyses. In the meantime, improved analyses, such as that presented here, will improve the extraction of information from gravity data and advance our understanding of subsurface mass movement.

ACKNOWLEDGEMENTS

Two anonymous reviewers provided insightful and effective comments. Benjamin Creutzfeldt and Andreas Güntner were critical in establishing the SAVSARP gravity project. Dan Winester, National Geodetic Survey, provided absolute-gravity measurements for calibrating the continuously recording gravimeters. GFZ-Potsdam, GWR Instruments, Inc. and Micro-g Lacoste, Inc. are gratefully acknowledged for providing instrumentation loans and project support. The project was supported by NSF grant EAR-1246619 and by the USGS Groundwater Resources Program. All data presented in the paper are available in the online repository ScienceBase at http://go.usa.gov/375Gm.

REFERENCES

Alnes, H., Eiken, O. & Stenvold, T., 2008. Monitoring gas production and injection at the Sleipner field using time-lapse gravimetry, *Geophysics,* **73**(6), WA155–WA161.

Anderson, J.M., Anderson, J.M. & Mikhail, E.M., 1998. *Surveying, Theory and Practice,* McGraw-Hill Science/Engineering/Math, p. 1200.

Battaglia, M., Gottsmann, J., Carbone, D. & Fernández-Álvarez, J.P., 2008. 4D volcano gravimetry, *Geophysics,* **73**(6), WA3–WA18.

Binley, A., Hubbard, S.S., Huisman, J.A., Revil, A., Robinson, D.A., Singha, K. & Slater, L., 2015. The emergence of hydrogeophysics for improved understanding of subsurface processes over multiple scales, *Water Resour. Res.,* **51**(6), 3837–3866.

Bonvalot, S., Diament, M. & Gabalda, G., 1998. Continuous gravity recording with Scintrex CG-3 M meters: a promising tool for monitoring active zones, *Geophys. J. Int.,* **135,** 470–494.

Brooks, R.J. & Corey, A.T., 1964. Hydraulic properties of porous media, Hydrol. Pap. 3, Color. State Univ. Fort Collins.

Brown, J.M., Niebauer, T.M., Richter, B., Klopping, F., Valentine, J.G. & Buxton, W.K., 1999. A new miniaturized absolute gravimeter developed for dynamic applications, *EOS, Trans. Am. geophys. Un.,* **80**(32), 355.

Chapman, D.S., Sahm, E. & Gettings, P., 2008. Monitoring aquifer recharge using repeated high-precision gravity measurements: a pilot study in South Weber, Utah, *Geophysics,* **73**(6), WA83–WA93.

Christiansen, L., Haarder, E.B., Hansen, A.B., Looms, M.C., Binning, P., Rosbjerg, D., Andersen, O.B. & Bauer-Gottwein, P., 2011a. Calibrating vadose zone models with time-lapse gravity data, *Vadose Zone J.*, **10,** 1034–1044.

Christiansen, L., Lund, S., Andersen, O.B., Binning, P., Rosbjerg, D. & Bauer-Gottwein, P., 2011b. Measuring gravity change caused by water storage variations: performance assessment under controlled conditions, *J. Hydrol.,* **402,** 60–70.

Creutzfeldt, B., Güntner, A., Klügel, T. & Wziontek, H., 2008. Simulating the influence of water storage changes on the superconducting gravimeter of the Geodetic Observatory Wettzell, Germany, *Geophysics,* **73**(6), WA95–WA104.

Crossley, D., Hinderer, J. & Riccardi, U., 2013. The measurement of surface gravity, *Rep. Prog. Phys.,* **76,** 046101, doi:10.1088/0034-4885/76/4/046101.

Ferguson, J., Chen, T., Brady, J.L., Aiken, C.L. & Seibert, J.E., 2007. The 4D microgravity method for waterflood surveillance. II—Gravity measurements for the Prudhoe Bay reservoir, Alaska, *Geophysics,* **72,** I33–I43.

Ferré, T.P.A. *et al.*, 2009. Critical steps for the continuing advancement of hydrogeophysics, *EOS, Trans. Am. geophys. Un.,* **90**(23), 200–202.

Furuya, M., Okubo, S., Sun, W., Tanaka, Y., Oikawa, J., Watanabe, H. & Maekawa, T., 2003. Spatiotemporal gravity changes at Miyakejima Volcano, Japan: Caldera collapse, explosive eruptions and magma movement, *J. geophys. Res.,* **108**(B4), 2219, doi:10.1029/2002JB001989.

Gettings, P., Chapman, D.S. & Allis, R.G., 2008. Techniques, analysis, and noise in a Salt Lake Valley 4D gravity experiment, *Geophysics,* **73**(6), WA71–WA82.

Hector, B., Séguis, L., Hinderer, J., Cohard, J.-M., Wubda, M., Descloitres, M., Benarrosh, N. & Boy, J.-P., 2015. Water storage changes as a marker for base flow generation processes in a tropical humid basement catchment (Benin): insights from hybrid gravimetry, *Water Resour. Res.,* **51,** 8331–8361.

Hwang, C., Wang, C. & Lee, L., 2002. Adjustment of relative gravity measurements using weighted and datum-free constraints, *Comput. Geosci.,* **28,** 1005–1015.

Jacob, T., Chery, J., Bayer, R., Le Moigne, N., Boy, J.-P., Vernant, P. & Boudin, F., 2009. Time-lapse surface to depth gravity measurements on a karst system reveal the dominant role of the epikarst as a water storage entity, *Geophys. J. Int.,* **177,** 347–360.

Jacob, T., Bayer, R., Chery, J. & Le Moigne, N., 2010. Time-lapse microgravity surveys reveal water storage heterogeneity of a karst aquifer, *J. geophys. Res.,* **115**(B6), B06402, doi:10.1029/2009JB006616.

Kennedy, J.R., 2015. Gravity data from the Sierra Vista subwatershed, Upper San Pedro Basin, Arizona, *Open-File Rep, U.S. Geol. Surv.,* 26, **2015-1086,** doi:10.3133/ofr20151086.

Kennedy, J.R., Ferré, T.P.A., Guntner, A., Abe, M. & Creutzfeldt, B., 2014. Direct measurement of subsurface mass change using the variable baseline gravity gradient method, *Geophys. Res. Lett.,* **41,** 2827–2834.

Krieg, L.A., 1981. Mathematical modelling of the behavior of the Lacoste and Romberg "G" gravity meter for the use in gravity network adjustments and data analyses, *Rep Dept. Geod. Sci. Surv. Ohio State Univ.,* **321,** 172.

LaCoste, L.J.B., 1988. The zero-length spring gravity meter, *Leading Edge,* **7**(7) 20–21.

Leirião, S., He, X., Christiansen, L., Andersen, O.B. & Bauer-Gottwein, P., 2009. Calculation of the temporal gravity variation from spatially variable water storage change in soils and aquifers, *J. Hydrol.,* **365,** 302–309.

Long, L.T. & Kaufmann, R.D., 2013. *Acquisition and Analysis of Terrestrial Gravity Data,* Cambridge University Press, p. 179.

MacMillan, W.D., 1958. *The Theory of the Potential,* Dover, p. 469.

Nagy, D., 1966. The gravitational attraction of a right rectangular prism, *Geophysics,* **31**(2), 362–371.

Naujoks, M., Kroner, C., Weise, A., Jahr, T., Krause, P. & Eisner, S., 2010. Evaluating local hydrological modelling by temporal gravity observations and a gravimetric three-dimensional model, *Geophys. J. Int.,* **182,** 233–249.

Niswonger, R.G., Panday, S. & Ibaraki, M., 2011. MODFLOW-NWT, a Newton formulation for MODFLOW-2005, *U.S. Geol. Surv. Tech. Methods,* **6-A37,** 44.

Niswonger, R.G., Prudic, D.E. & Regan, R.S., 2006. Documentation of the unsaturated-zone flow (UZF1) package for modeling unsaturated flow between the land surface and the water table with MODFLOW-2005, *U.S. Geol. Surv. Tech. Methods,* **6-A19,** 62.

Pfeffer, J. *et al.*, 2013. Evaluating surface and subsurface water storage variations at small time and space scales from relative gravity measurements in semiarid Niger, *Water Resour. Res.,* **49,** doi:10.1002/wrcr.20235.

Pool, D.R., 2008. The utility of gravity and water-level monitoring at alluvial aquifer wells in southern Arizona, *Geophysics,* **73**(6), WA49–WA59.

Pool, D.R. & Eychaner, J.H., 1995. Measurements of aquifer-storage change and specific yield using gravity surveys, *Ground Water,* **33**(3), 425–432.

Schmerge, D. & Francis, O., 2006. Set standard deviation, repeatability and offset of absolute gravimeter A10-008, *Metrologia,* **43,** 414–418.

Schmerge, D. *et al.*, 2012. Results of the first North American comparison of absolute gravimeters, NACAG-2010, *J. Geod.,* **86,** 591–596.

Sugihara, M. & Ishido, T., 2008. Geothermal reservoir monitoring with a combination of absolute and relative gravimetry, *Geophysics,* **73**(6), WA37–WA47.

Torge, W., 1989. *Gravimetry,* De Gruyter.

Torge, W., 2001. *Geodesy,* 3rd ed., De Gruyter.

Touati, F., Kahlouche, S. & Idres, M., 2010. Robust and efficient weighted least squares adjustment of relative gravity data, in *Gravity, Geoid, and Earth Observation,* International Association of Geodesy Symposia, pp. 59–65, ed. Mertikas, S.P., Springer, Berlin Heidelberg.